Experimental Mechanics (2011) 51:1421–1433
DOI 10.1007/s11340-010-9462-z

Multiaxial Mechanical Characterization of Interpenetrating Polymer Network Reinforced Acrylic Elastomer

A. Schmidt · A. Bergamini · G. Kovacs · E. Mazza

Received: 2 November 2010 / Accepted: 27 December 2010 / Published online: 17 February 2011
© Society for Experimental Mechanics 2011

Abstract The acrylic elastomer membrane VHB 4910 is a material widely used for applications as Dielectric Elastomer Actuators DEA. For suitable actuation performance however, it is necessary to pre-strain the very compliant membrane. This reduces the lifetime of DEA due to early failure of the tensioned membrane. Interpenetrating Polymer Network Reinforced Acrylic Elastomers (IPN) are produced by introducing a curable additive into the pre-strained acrylic elastomer membrane. While curing at elevated temperature, the additive forms a second polymeric network that supports part of the pre-strain in the acrylic membrane. This leads to a free standing material that combines the actuation performance of pre-strained VHB 4910 with an excellent long-term reliability. This work presents a detailed mechanical characterization of acrylic IPN membranes. To reduce the experimental effort required to characterize the nonlinear elastic behavior, we developed a unique specimen design that enables the assessment of uni- and biaxial stress states within one experiment. Slight changes in the material composition of IPN-membranes lead to substantial variations in their mechanical properties. The extraction of material behavior in different kinematic states within a single sample thus reduces the uncertainty on the determination of constitutive models. An extensive experimental campaign was carried out involving uniaxial and equibiaxial tension and relaxation. Image based local deformation measurements and iterative finite element calculations were applied to derive constitutive model parameters that describe the mechanical response in a wide range of planar strain and strain rate.

Keywords Multiaxial · Biaxial · Elastomer · IPN · Characterization

A. Schmidt (✉) · A. Bergamini · G. Kovacs · E. Mazza
Swiss Federal Laboratories for Materials
Testing and Research (Empa),
8600 Dübendorf, Switzerland
e-mail: schmidt@imes.mavt.ethz.ch

A. Schmidt · E. Mazza
Department of Mechanical and Process Engineering,
Swiss Federal Institute of Technology (ETH),
8092 Zürich, Switzerland

Introduction

Dielectric Elastomer Actuators (DEA) are made of a soft polymeric membrane coated on opposite sides with a compliant layer of conductive material. The conductive material serves as electrodes that, if subjected to a voltage, lead to an electrical field across the membranes. As a consequence, the dielectric membrane contracts in thickness direction and expands in-plane. Both the thickness contraction as well as the in-plane expansion can be used for actuation. Studies on acrylic elastomers showed that pre-straining the membrane significantly increases the performance of such actuators [1–3]. The introduction of Interpenetrating Polymer Networks (IPN) to acrylic DEA by *Ha* et. al. [4] led to a material that offers the performance of pre-strained acrylic elastomers without the need of externally supported pre-strain. Using this material, *Kovacs* et al. [5] developed a free standing contractile actuator that directly uses the out-of-plane contraction. This leads to very high actuation forces while the absence of external pre-strain significantly enhances the reliability.

In general a electromechanical model suitable for actuator simulation and design optimization is necessary for this material system. Such a model has to predict the nonlinear materials response in different kinematic states

and for different strain rates. So far, there have been different approaches to derive electromechanical models of DEA. Many authors characterized the passive mechanical material response with simple quasi-static uniaxial tensile tests [6–9]. The pronounced viscoelasticity of most DEA-materials was investigated with uniaxial relaxation [10–12] or creep tests [13]. A reliable prediction of the response to compression in thickness direction with a phenomenological model derived from in plane uniaxial tensile tests seems rather unlikely for nonlinear materials. Therefore more recently DEA-models were determined by fitting mechanical model parameters to the results of experiments with actuators [14–16]. While this seems more appropriate for mechanically nonlinear materials the approach relies on the knowledge of the electromechanical coupling mechanism. The model of an "ideal" dielectric adopted so far for describing electromechanical coupling [17] was recently shown to be questionable, due to neglected electrostrictive effects [18]. To test and verify the different electromechanical coupling models, purely mechanical experiments are therefore necessary.

Specifically on the mechanical characterization of IPN not much work was reported so far. *Ha* et al. [19] conducted membrane inflation tests with IPN films of different material compositions and showed a strong dependence of elastic response from the amount of additive forming the second network. Only values of the tangent modulus are reported and no time-dependence was considered. In a later paper, *Ha* et al. [12] compared two different IPN formulations based on VHB 4910 and VHB 4905 with different amounts of additive and determined time-dependent hyperelastic parameters from uniaxial relaxation experiments. These model parameters have not been verified using experiments with multiaxial stress states or actuators. *Düring* [20] derived hyperelastic parameters from membrane inflation tests with IPN but neglected time-dependence. This model only reproduces the behavior observed in so called stacked actuators for very low activation voltages.

In this work we present a detailed mechanical characterization of IPN membranes. For the presented test campaign, IPN membranes were produced from pre-strained VHB 4910 membranes by introducing the trifunctional acrylic *Trimethylolpropane trimethacrylate* (TMPTMA) into the membrane. At a temperature of 85° C, this additive forms an additional polymeric network that effectively supports part of the pre-strain when the external boundary condition is removed. While the applied pre-strain of 400% undergoes only minor variations in the fabrication process, the amount of functional additive can change due to process uncertainties. Different amounts of additive will lead to a different stiffness of the secondary network, thus to different levels of preserved pre-strain and membrane thickness (Fig. 1), and correspondingly to a different tangent modulus of the base elastomer [4, 11]. These mechanisms were recently investigated by *Zhu* and *Suo* [21], who proposed a model for the interaction of the 2 polymer networks.

Differently from the approach proposed in [21], we do not develop physically or microstructural based models in this work. Instead we intend to provide phenomenological equations with corresponding model parameters fitting the experimental data, which can be used for finite element (FE) based design and optimization of IPN actuators. Different strain energy formulations are compared in their capability of describing the material response in multiple deformation states.

Since an equibiaxial tensile stress in the membrane plane leads to the same kinematics of deformation as a uniaxial compression perpendicular to the membrane for isotropic materials, and since the uniaxial compression as occurring in an actuator is very difficult to be realized in a mechanical experiment with very thin and sticky membranes, equibiaxial tensile tests were selected here to derive constitutive models for DEA.

We performed a large number of equibiaxial and uniaxial tensile tests and all measurement results are reported here. A relatively large scatter was observed for the results of the experiments. This scatter was found not to be due to measurement uncertainties but to process induced variations in material composition. In fact the membranes tested had different undeformed thicknesses and thus a different material composition. However, only membranes with identical material composition can be expected to reveal a similar mechanical response. For membranes with a different material composition a membrane specific constitutive model is required. In order to obtain sample specific information on the multiaxial behavior of an IPN membrane we developed a specimen design that allows the determination of the materials response in both biaxial and uniaxial tension within one experiment on one sample.

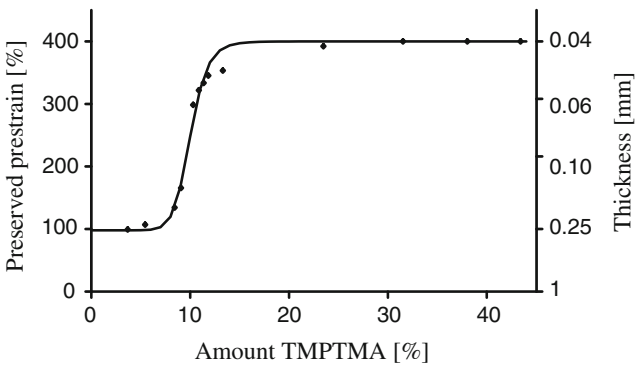

Fig. 1 Measured preserved pre-strain [19], model fit and calculated membrane thickness vs. amount of functional additive

Further we propose an approach to account for the material composition dependence of the mechanical response and included a corresponding correction term into the constitutive model. This approach is shown to effectively reduce deviations between experimental results and model predictions.

Experiments

Nonlinear and time dependent mechanical behavior of DEA materials can be modeled using hyperelastic viscoelastic constitutive laws. A strain energy density function has to be determined from which the components of the stress tensor can then be derived by calculating the partial derivative of the strain energy density function with respect to the corresponding deformation measure. Typically a large number of parameters are incorporated in common strain energy formulations. The determination of these parameters requires a considerable experimental effort. To ensure an accurate prediction of the material response the experimental characterization should include experiments over a wide range of strain states and strain rates. We conducted biaxial and uniaxial relaxation for different strain values and strain rates.

An overview of all experiments with corresponding sample number and membrane thickness is given in Table 1. Since the undeformed thickness of the base membrane VHB 4910 is always 1 mm, the existence of different IPN membrane thicknesses gives evidence that in fact variations in material composition do occur. For the samples tested in biaxial relaxation the amount of TMPTMA was around 12 wt%. The influence of the amount of additive on the preserved pre-strain is very strong in this range (Fig. 1). Very small variations in material composition can therefore cause a significant scatter in the results of mechanical testing.

Table 1 Overview of experiments and samples

Test condition	Sample	Thickness [μm]
Biaxial control profile 1	1_1	69
Biaxial control profile 1	1_2	71
Biaxial control profile 2	2_1	66
Biaxial control profile 2	2_2	64
Biaxial control profile 2	2_3	65
Biaxial control profile 3	3_1	67
Biaxial control profile 3	3_2	70
Biaxial control profile 4	4_1	67
Biaxial control profile 4	4_2	68
Uniaxial relaxation	5_1	67
Uniaxial relaxation	5_2	67
Uniaxial relaxation	5_3	68
Uniaxial relaxation	5_4	72
Uniaxial relaxation	5_5	72
Uniaxial relaxation	5_6	73
Uniaxial relaxation	5_7	83
Uniaxial relaxation	5_8	86
Uniaxial relaxation	5_9	87
Uniaxial relaxation	5_10	88
Uniaxial relaxation	5_11	89
Uniaxial relaxation	5_12	92
Uniaxial relaxation	5_13	93
Uniaxial relaxation	5_14	95

Biaxial Experiments

The biaxial relaxation experiments were performed at room temperature (23°C) on a biaxial tensile testing device at ETH Zurich. The device offers separately controlled displacement and force measurement on four actuators. The deformation is measured locally on the specimens with an image based grey scale correlation technique. Unlike in uniaxial tests, the measured force signals of biaxial experiments in general do not allow a direct calculation of the stress values in the specimen. In fact, depending on the geometry of the testpiece, the stress state can be highly inhomogeneous. Various approaches were proposed for optimization of sample geometry in order to reduce the complexity of the inverse problem [22–29]. For IPN membranes the application of tensile loads using wires and hooks is not feasible due to material sensitivity to notches. A cruciform specimen design is used here, with five slots introduced on each arm (Fig. 2). These slots effectively reduce the influence of the transition from the uniaxial stress state of the arm to the equibiaxial zone in the center [30]. Further, a cruciform design offers information on the uni- and the biaxial response at the same time. By measuring the deformation in the biaxial domain, as well as the displacement at the clamping points, the strain state can be determined for both domains.

To ensure repeatable test conditions we punched our cruciform specimens out of membranes with the dimensions indicated in Fig. 2. A special mounting frame is used to clamp the specimens at the four actuators in the undeformed configuration. In all different experiments a displacement ramp was applied to each actuator. In total four different equibiaxial experiments each involving the test of at least two specimens were performed. The control profile shown in Fig. 3 represents the applied displacement U(t) for all four experiments.

Uniaxial Experiments

In addition to the extraction of uniaxial data from the uniaxial domain of the biaxial experiments, uniaxial relaxation experiments with samples of different thickness

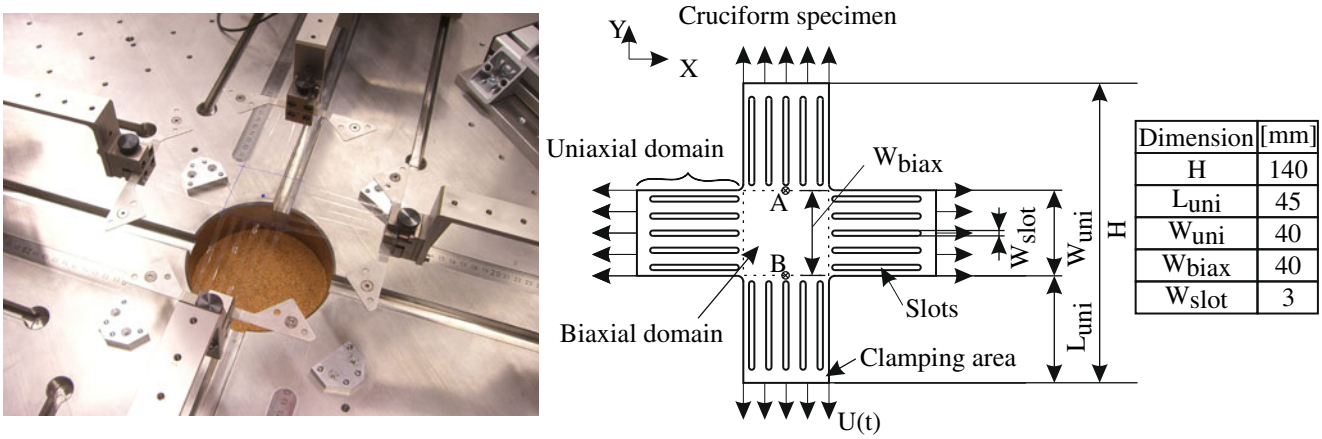

Fig. 2 Biaxial tensile testing device and cruciform specimen

were performed. All of these uniaxial experiments were carried out using one axis of the biaxial tensile testing device. The specimens were cut to a length of 90 mm and a width of 9 mm. All different specimens were stretched to a nominal strain of 100 % within 10 s and held in this position for 300 s. Strain rate and duration of dwell time were chosen to be in a range relevant for cyclic applications in actuators see e.g. [31, 32] and close to the values observed in the biaxial experiments.

Results

Results of Biaxial Experiments

The stretches in x and y-direction given in Fig. 4 are derived from the image analysis procedure and relate the deformed width of the biaxial domain w_{biax} to the undeformed width W_{biax} (see Fig. 2). Thus the stretch values indicate an average value of relative deformation of the domain between points A and B. Since the same displacement is applied to all 4 actuators all curves in each diagram of Fig. 4 should be identical. Deviations between stretches are in the range of 10 %. Despite the application of a linear time ramp for U(t) (Fig. 2) the results reveal a somewhat nonlinear stretch ramp in the biaxial domain visible in particular in the case of exp. 4. This is the consequence of a different stiffness in uni- and biaxial domain. As Fig. 4 also shows, there is almost no follow up and the stretch is constant during the hold time. From biaxial stretch and applied displacement U(t) the stretch in the uniaxial domain is calculated (Fig. 5). Note that in all experiments the uniaxial stretch is much larger than the biaxial deformation. Figure 6 shows the tensile force separately for each sensor in each experiment. As expected, the signals of all sensors almost coincide, revealing no sign of anisotropy in the specimens as well as high measurement accuracy. Further Fig. 6 shows the averaged force signal of four sensors for each specimen. Since the samples had different thicknesses, the scatter of tensile force between the specimens of each experiment (Fig. 6 right) will be evaluated on the basis of calculated stress values in "Analysis".

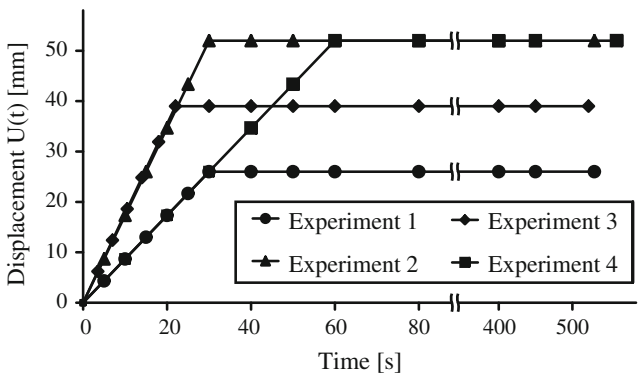

Fig. 3 Actuator displacement control profiles of biaxial relaxation experiments U(t)

Results of Uniaxial Relaxation Experiments

Uniaxial relaxation experiments were performed on samples with significant differences in their thickness (see Table 1) and thus different material composition. All experiments were performed with the same strain ramp of 100 % nominal strain in 10 s and subsequently a stress relaxation with constant strain for more than 300 s. The significant dependence of mechanical response on material thickness becomes evident in these experiments, see Fig. 7. Cauchy stress values were calculated from measured force and stretch values assuming incompressible behavior. The membranes with larger additive content and therefore smaller thickness are considerably stiffer than the samples with low additive content. Both peak stresses as well as long term stresses vary by a factor of about 3. Note the

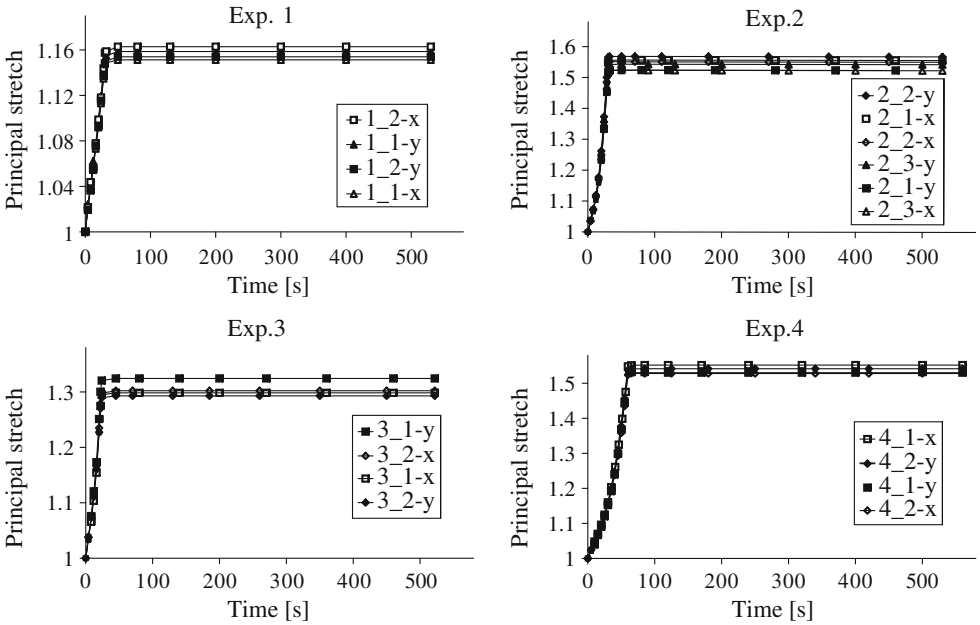

Fig. 4 Principal stretches in the biaxial domain (sample numbers according to Table 1, legend lists curves from large to small values of stretch)

deviation of more than 20 % in peak stress between the membranes of 0.067 and 0.072 mm.

Analysis

Material Model Formulations

Three strain energy formulations were compared in their capabilities of representing uniaxial as well as biaxial response. For all models incompressible behavior was assumed (Poisson's ratio υ=0.5), which represents a common hypothesis when modeling the mechanical behavior of elastomers. The *Reduced Polynomial* or *Yeoh*-model [33] calculates the strain energy dependent on the first invariant I_1 of the left Cauchy-Green strain tensor. This objective measure of relative deformation is calculated from the so called principal stretches λ_i.

$$I_1 = \lambda_1^2 + \lambda_2^2 + \lambda_3^2 \tag{1}$$

$$W = \sum_{i=1}^{3} C_i (I_1 - 3)^i \tag{2}$$

Three material parameters C_1, C_2 and C_3 have to be determined from experimental data.

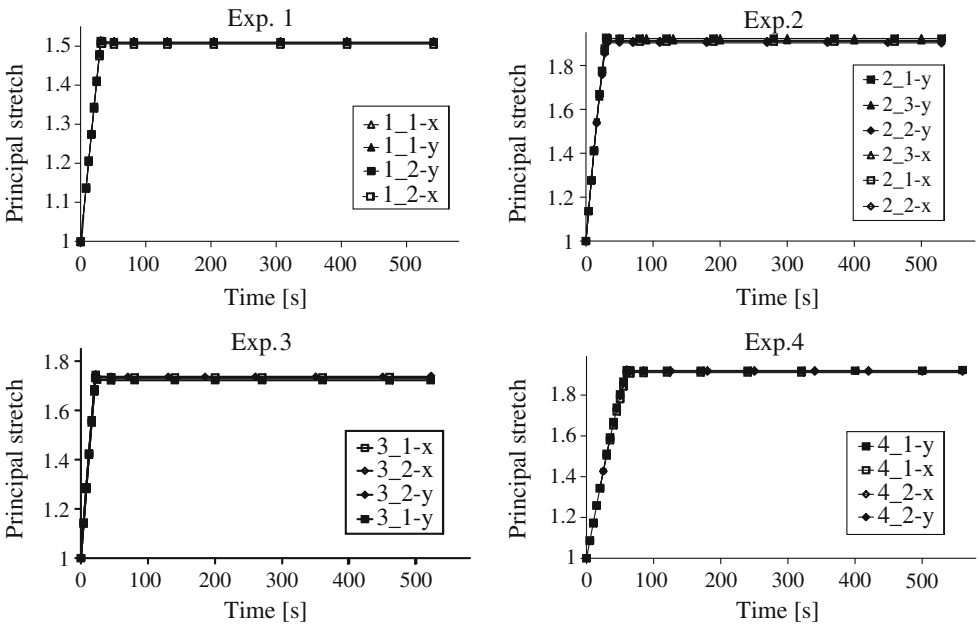

Fig. 5 Principal stretches in the uniaxial domain (sample numbers according to Table 1, legend lists curves from large to small values of stretch)

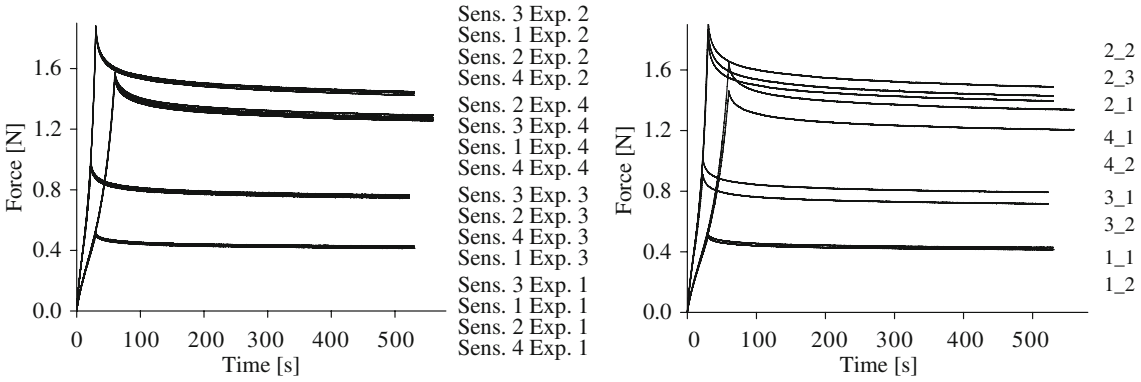

Fig. 6 Typical measurement of tensile force on each sensor for selected samples (left) and average force for each sample (right), (legend lists curves from large to small values of force)

The *Ogden*-model [34] expresses the strain energy directly as a function of the principal stretches. In the following a three term *Ogden*-model is used:

$$W = \sum_{j=1}^{3} \frac{2\mu_j}{\alpha_j^2}\left(\lambda_i^{\alpha_j} - 3\right) \tag{3}$$

It should be noted that this form is different from the one originally proposed by *Ogden* but it coincides with the formulation implemented in the general purpose FE software *ABAQUS*. The material parameters μ_i and α_i need to be determined from experiments. The *Arruda-Boyce*-model [35] is based on statistical mechanics and requires the determination of only two different material parameters: μ and λ_m.

$$W = \mu \cdot \left[\frac{1}{2}(I_1 - 3) + \frac{1}{20\lambda_m^2}\left(I_1^2 - 9\right) + \frac{11}{1050\lambda_m^4}\left(I_1^3 - 27\right) + \frac{19}{7000\lambda_m^6}\left(I_1^4 - 81\right) + \frac{519}{673750\lambda_m^8}\left(I_1^5 - 243\right)\right] \tag{4}$$

Assuming quasi-linear viscoelasticity for the description of time dependent mechanical behavior [11], the coefficients of the strain energy functions (C_i, μ_i and μ respectively) are expressed as a function of time and are multiplied with the relaxation function *g(t)*

$$g(t) = 1 - \sum_{k=1}^{4}\left[1 - \exp\left(\frac{t}{-t_k}\right)\right] \tag{5}$$

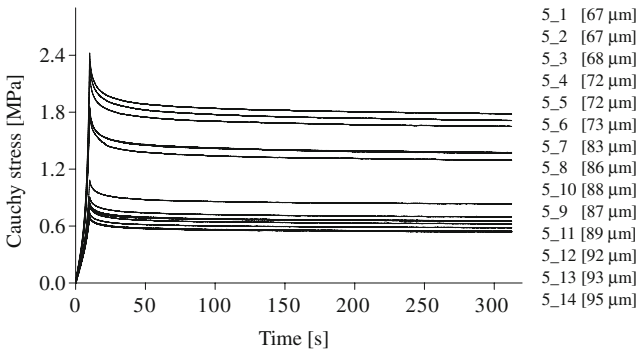

Fig. 7 Cauchy stress in uniaxial relaxation for IPN-membranes of different thickness (the thickness is reported in brackets after the sample number, legend lists curves from large to small values of stress)

Simplified Stress determination for the Biaxial Experiments

To achieve reliable predictions of the mechanical response for strains up to 50 %, in both uniaxial and multiaxial loading, the models were fitted simultaneously considering uni- as well as biaxial domains of the four biaxial experiments. In theory this can be accomplished by applying the experimental displacement on a detailed FE model of the cruciform specimen. With the help of optimization algorithms the deviation of experimental and calculated tensile force can be minimized by adapting the material parameter. This process however involves extensive computational costs.

A different approach was used here. The cruciform specimen design with five slots in each of the uniaxial domains (Fig. 2) effectively reduces the influence of the transition between pure uniaxial and equibiaxial stress state. For an ideal transition the principal true or Cauchy-stress values are identical to the nominal stress calculated from measured tensile force F and deformed cross-sectional area a.

$$\sigma_H = \frac{F}{a} \tag{6}$$

Assuming an incompressible material behavior in an equibiaxial stress state,

$$\lambda_1\lambda_2\lambda_3 = 1 \tag{7}$$

$$\lambda_3 = \frac{1}{\lambda_1\lambda_2} = \frac{1}{\lambda^2} \tag{8}$$

the deformed cross-sectional area can be calculated from undeformed cross-sectional area A and principal stretch λ of the biaxial region.

$$a = w_{biax} \cdot d = W_{biax} \cdot \lambda \cdot \frac{D}{\lambda^2} = \frac{W_{biax} \cdot D}{\lambda} = \frac{A}{\lambda} \tag{9}$$

FE calculations were performed to compare the Cauchy stress within the biaxial region with the prediction from equation (6) (idealized transition). This comparison allowed determining a correction factor (κ) for the simplified analysis of the biaxial experiments:

$$\sigma_B = \kappa \cdot \sigma_H \tag{10}$$

with σ_B as the Cauchy stress to be used for a homogenized model considering non-ideal transition at the interface between uniaxial and biaxial domain. Figure 8 shows the deformed biaxial domain of the FE model of sample 1_2. The color plot shows the stress-ratio σ_{FE}/σ_H with σ_{FE} as the maximum principal stress from the FE calculation. The value of κ is calculated from the average stress-ratio of all elements in the biaxial region. Thereto different material model formulations were compared. For the models reported in Table 2, κ takes values between 0.849 and 0.861.

Values of Cauchy stress σ_B were calculated according to equations (6), (9) and (10) with κ=0.85 for the biaxial region, see Fig. 9.

Similarly, an effective length of the uniaxial domain was calculated from a detailed FE model, thus allowing the calculation of an approximated value of Cauchy stress in the uniaxial region. This approach leads to simplified models of the experiment (Fig. 10). The fitting process for the determination of the hyperelastic viscoelastic material model parameter is realized with a *Matlab* routine including the optimization tool *fminsearch* that uses the simplex search method of [36]. This routine passes an initial material parameter set into *ABAQUS*. The measured deformation of the uniaxial and biaxial domain is applied to the simplified FE models for each time increment. The calculated stress values are then compared with the measurements and the value of the objective function is determined. By iteratively varying the parameter of the material model the value of the objective function is minimized.

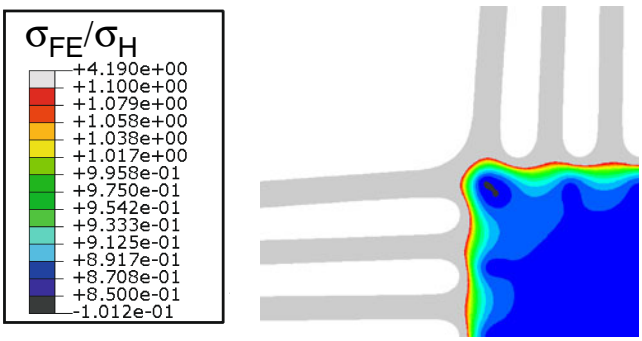

Fig. 8 Ratio of principal stress σ_{FE}/σ_H (λ=1.15)

Table 2 Hyperelastic material parameters

Yeoh	C_1 [MPa]	C_2 [MPa]	C_3 [MPa]			
	0.219	0.058	-0.0007			
Ogden	μ_1 [MPa]	μ_1 [MPa]	μ_1 [MPa]	a_1	a_3	a_3
	0.277	0.330	-0.248	-1.037	7.222	7.222
Arruda-Boyce	μ [MPa]	λ_m				
	0.260	1.313				

Material Model Parameters

The fitting process was accomplished for all three hyperelastic viscoelastic models, leading to the parameters given in Tables 2 and 3. In Fig. 11 the experimental results, regarded as average of data from the (2 or 3) samples of each experiment, are compared with the model predictions for the biaxial and uniaxial material response. As can be seen all three material model formulations give fairly accurate predictions of the biaxial response in experiment 1 and 3 but deviate from the measured values for experiment 2 and 4. For the uniaxial material response the constitutive model predictions are in general less reliable. Further we observe better results using the *Ogden*-model.

There is an obvious difference in the response for the different specimens of each experiment as shown by the

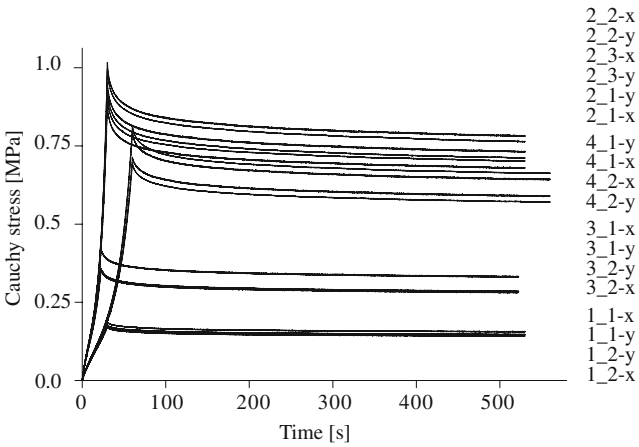

Fig. 9 Approximate histories of Cauchy stress σ_B in the biaxial domain (sample number according to Table 1, curves listed from large to small values of stress)

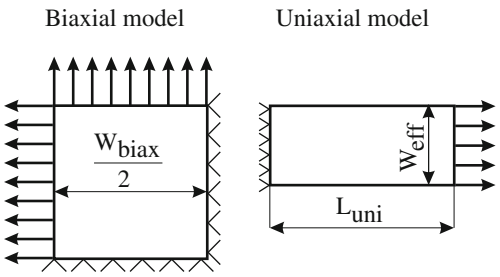

Fig. 10 Simplified FE models

results of Fig. 9. As anticipated in the introduction, we suggest that differences in material composition lead to different mechanical properties. This interpretation would explain the reason for the discrepancy between models and experiments in Fig. 1. In fact for each membrane a specific parameter set should be used. In chapter 4 we will further discuss this problem and derive an expression accounting for the material composition. Naturally, repeated experiments with samples of an identical material composition and thus the same thickness are necessary to characterize the material. However the difference in material composition of a membrane of 0.064 and one of 0.07 mm thickness is so small (compare Fig. 1) that it cannot be avoided in the production process. Therefore the material might be considered as identical and a scatter of up to 20% in mechanical testing is then observed. As we will show in the following, most of this apparent scatter can essentially be attributed to variations in material composition and thus does not represent an experimental uncertainty but a materials property that can be characterized.

Constitutive Model Formulation Considering Material Composition

Model Formulation

As explained in the introduction, different material compositions lead to a different level of preserved pre-strain of the VHB membrane and thus to a different thickness of the IPN membrane. Within the range of 0.06-0.1 mm the material can be used for dielectric actuation. Membranes below this thickness experience only small active strains due to their relatively large stiffness while membranes above 0.1 mm are very compliant but the small amount of preserved pre-strain limits the possible electrical field due to breakdown. Figure 7 shows the stress history in uniaxial relaxation experiments for membranes within this range of thickness. As can be seen the stiffness of these membranes varies by a factor of three. In the following we will propose an approach in order to account for these variations by a membrane specific constitutive model formulation.

Recently Zhu and Suo proposed a constitutive law that expresses the strain energy potential of IPN as the sum of potentials of both networks weighed with their respective volumetric fraction [21]. While this approach seems the most natural it relies on the assumption that no chemical cross-linking between both networks occurs and that the strain energy potentials of each network is not affected by IPN processing. In the specific case of IPN made from VHB 4910 and TMPTMA we are not able to exclude chemical cross-linking. Further it is not possible to experimentally assess the strain energy potential of the TMPTMA-network. In our phenomenological approach the strain energy potential of IPN is described by a function fitted to experimental data of membranes with different material composition. As can be concluded from Figs. 1 and 7, small differences in material composition lead to large variations in material stiffness within the range of membrane thickness suitable for actuation. Such small variations of the material composition cannot be controlled nor quantified in the production process.

For the system treated, the undeformed IPN membrane thickness is a measurable quantity that depends on material composition. Since the base elastomer VHB 4910 always possess an undeformed thickness of 1 mm and is always pre-strained to 400×400%, the undeformed thickness of the IPN membranes is directly linked to the material composition (Fig. 1). Therefore and unlike to other geometrical variables, the undeformed membrane thickness can in this case be used as a membrane specific parameter that relates the constitutive model parameter with those of a reference membrane. In contrast to the amount of secondary network, the undeformed membrane thickness is easily assessable with the necessary accuracy. We therefore use the undeformed IPN membrane thickness d as the variable that describes the dependence on the

Table 3 Parameter of the relaxation function

	g_1	t_1[s]	g_2	t_2[s]	g_3	t_3[s]	g_4	t_4[s]
Yeoh	0.325	0.03	0.141	3.75	0.106	7.60	0.048	141.7
Ogden	0.186	0.01	0.200	2.97	0.112	11.78	0.052	178.3
Arruda-Boyce	0.300	0.03	0.128	4.20	0.110	8.30	0.052	127.2

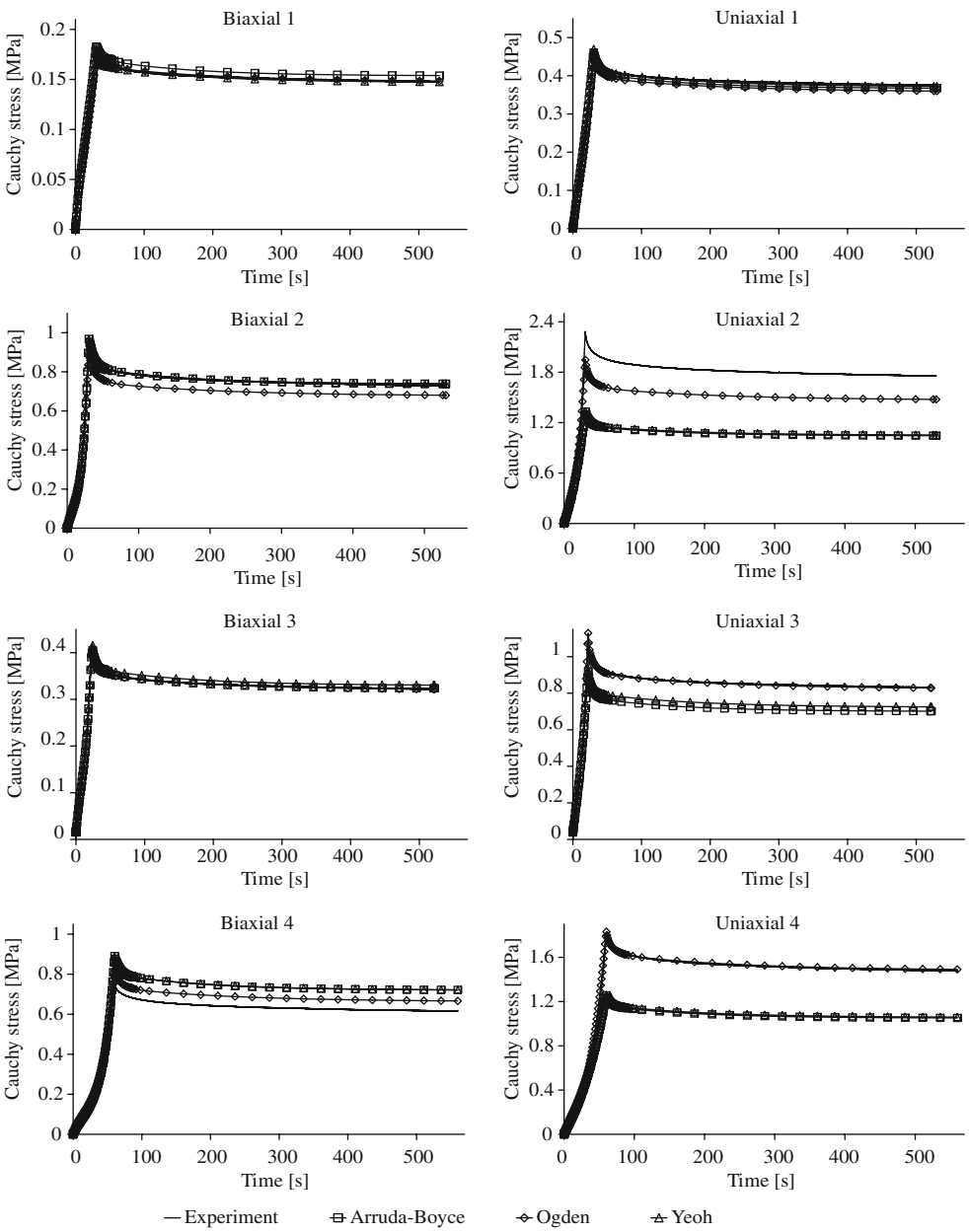

Fig. 11 Comparison of Cauchy stress histories calculated from experimental data and predictions of three material models for four different uni- and biaxial stress states

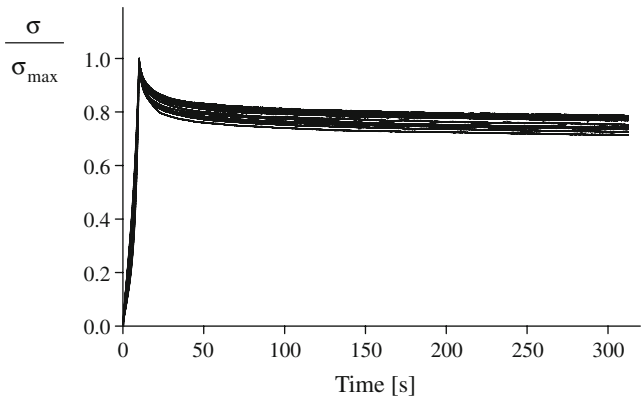

Fig. 12 Normalized stress in uniaxial relaxation

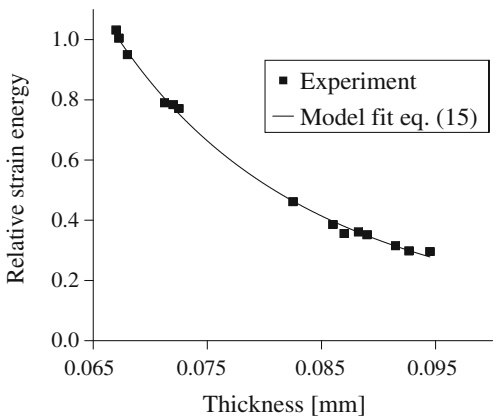

Fig. 13 Relative strain energy density of different samples and model fit (15)

Table 4 Parameter of the extended *Ogden*-model

$W(\lambda_i)$	μ_1 [MPa]	a_1	μ_2 [MPa]	a_2	μ_3 [MPa]	a_3		
	0.386	0.206	0.119	7.182	-0.066	6.397		
$f(d)$	d_0 [mm]	B						
	0.067	-3.76						
$g(t)$	g_1	t_1 [s]	g_2	t_2 [s]	g_3	t_3 [s]	g_4	t_4 [s]
	0.186	0.01	0.200	2.97	0.112	11.78	0.052	178.2

material composition. In agreement with the hypothesis of quasi-linear viscoelasticity, the relaxation functions are assumed to be strain independent. In fact, uniaxial relaxation experiments with different strain values up to 500 % confirmed this hypothesis for VHB 4910 [11]. We therefore propose that the general strain energy density function for the group of all IPN membranes produced according to the protocol described in [19] can be written as follows:

$$W(\lambda_i; t; d) = W(\lambda_i; d) \cdot g(t; d) \tag{11}$$

With the strain energy density as a function of the principal stretches, time and material composition in this case the undeformed membrane thickness. The relaxation curves from Fig. 7 are represented as normalized functions with respect to the maximum stress values σ_{max} in Fig. 12. The relatively low variability of these relaxation functions indicates that the specific material composition has a small influence on the time-dependence of the mechanical response. The low volume fraction of TMPTMA in the investigated IPN makes this observation plausible. This might lead to the conclusion that the observed dissipative behavior depends on the viscoelastic properties of the VHB network rather than on the TMPTMA component. In the model formulation, we assume the time-dependent part of the general strain energy density function to be independent

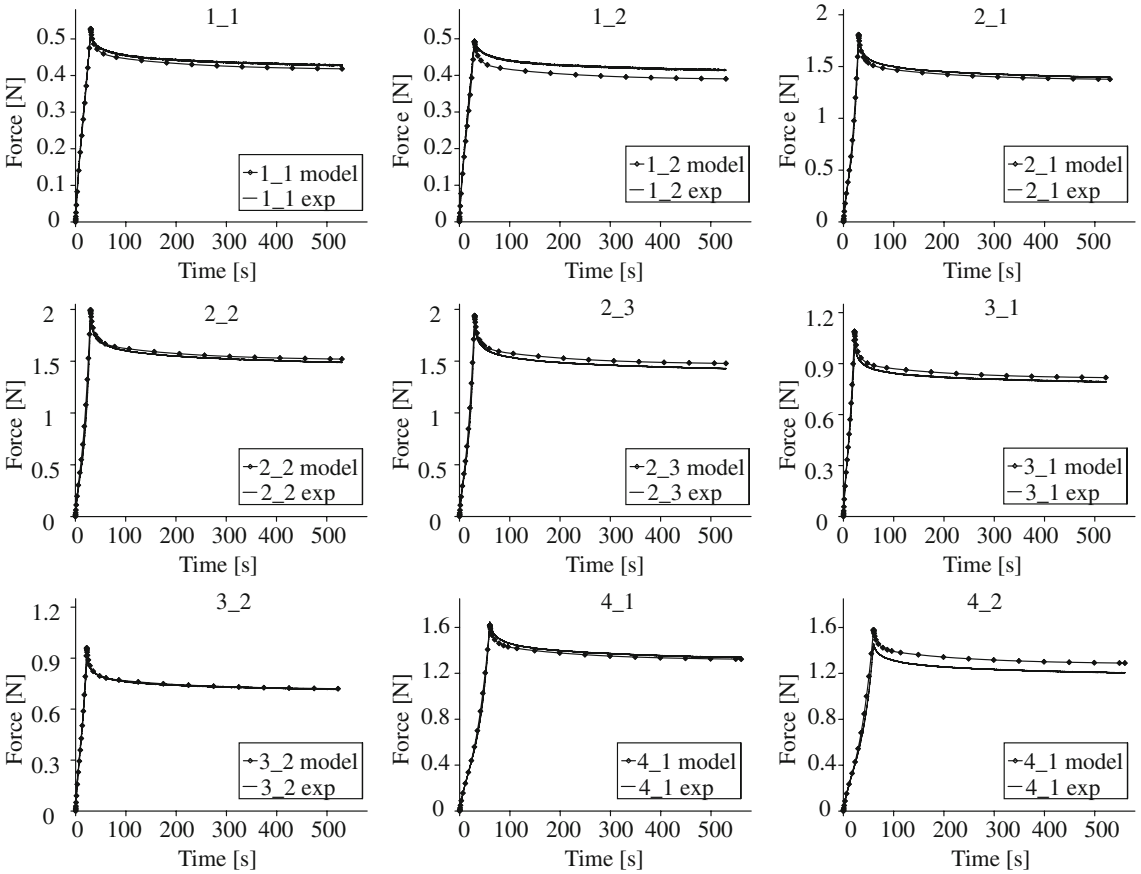

Fig. 14 Comparison of the predicted force histories of the detailed FE models (symbols) with the measured values for each experiment (lines)

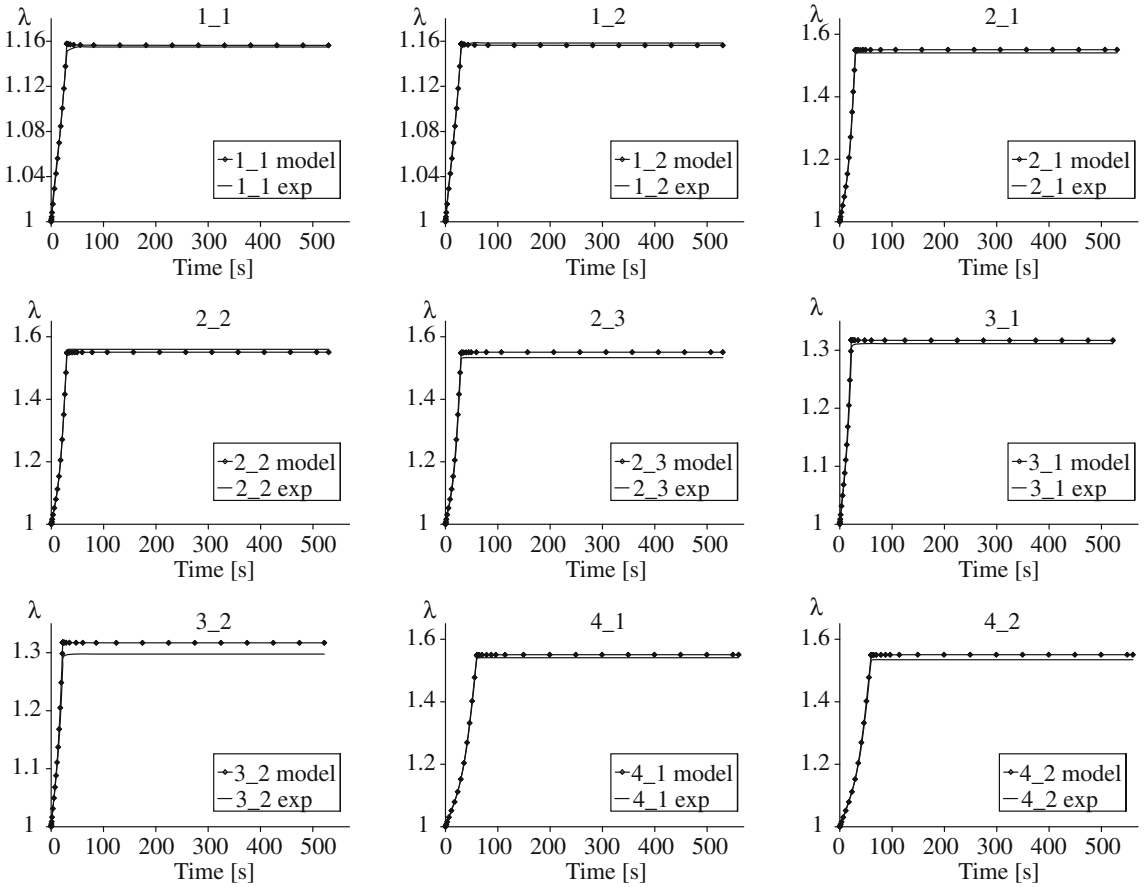

Fig. 15 Comparison of predicted and measured stretch histories in the biaxial domain

of thickness (and thus independent of the amount of TMPTMA):

$$W(\lambda_i;d)\cdot g(t;d) = W(\lambda_i;d)\cdot g(t) \tag{12}$$

In a first approach we further propose a simple multiplicative split of material composition dependence and deformation dependence, thus leading to:

$$W(\lambda_i;d)\cdot g(t) = W(\lambda_i)\cdot g(t)\cdot f(d) \tag{13}$$

The function *f(d)* only depends on the membrane thickness. Values of *f(d)* can therefore be determined by relating the strain energy density of individual membranes to the strain energy density of a reference membrane with thickness d_0 tested with the same strain history.

$$f(d) = \frac{W(\lambda_i,t,d)}{W(\lambda_i,t,d_0)} \tag{14}$$

Figure 13 shows this relative strain energy density derived for the peak stress values measured in uniaxial relaxation experiments (Fig. 7) as a function of the amount of TMPTMA and as a function of the membrane thickness. The data was fitted using a power law, see equation (15) with d_0=0.067 mm as the selected reference value of membrane thickness for which *f(d)*=1.

$$f(d) = \left(\frac{d}{d_0}\right)^B \quad d_0 = 0.067mm \quad B = -3.76 \tag{15}$$

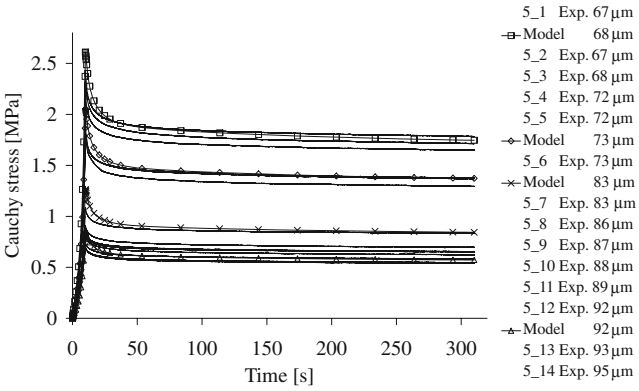

Fig. 16 Comparison of selected predictions of the stress histories with the measured values for uniaxial experiments, (legend lists curves from large to small values of stress)

Application to the Experimental Data

The fitting process described in chapter 3 was applied to each sample of the biaxial experiments, using for each membrane the corresponding value of the function *f(d)*, that simply scales the strain energy density of each membrane. We therefore introduce a corresponding specific set of coefficients μ_i of the Ogden-model for the FE simulation of each membrane. The new model formulation (Ogden form) and the corresponding parameters are reported in equation (16) and Table 4.

$$W(\lambda_i,d,t) = f(d)\cdot g(t)\cdot W(\lambda_i) = \left(\frac{d}{d_0}\right)^B \cdot \left(1-\sum_{k=1}^{4} g_k\left[1-e^{\left(\frac{-t}{\tau_k}\right)}\right]\right) \cdot \left(\sum_{j=1}^{3}\frac{\mu_j}{\alpha_j^2}\left(\lambda_i^{\alpha_j}-3\right)\right) \quad (16)$$

The calculated tensile forces of detailed FE models using the new material parameters are compared with the respective experimental data in Fig. 14. These detailed models were calculated with the software Abaqus 6.7-1. The models use eight node elements with quadratic interpolation (S8R) with a discretization level sufficient to ensure convergence of the results. For the detailed FE models the same displacement ramp was applied at the extremity of each arm as in the experiments. Thus the resulting stretch within the biaxial domain depends on the ratio of material stiffness in uniaxial and biaxial stress state. A comparison of measured and calculated stretch in the biaxial domain is given in Fig. 15. There is now an excellent agreement between model prediction and measurement for both force as well as stretch. The largest deviations are of the order of ±5 %. The film thickness measurement shows a variability in the order of ±1 μm. Within the correction function *f(d)* this translates to an uncertainty of material model parameters of ±5 % thus confirming the quality of the material model fit.

A comparison between measurement and predictions of the new model (equation 16) for the uniaxial experiments is shown in Fig. 16.

As expected since the correction function was determined from these data, there is an excellent agreement between experiments and simulations.

Conclusions

The proposed 3D hyperelastic viscoelastic model extends previous work on the mechanical characterization of IPN. We have reported data measured in a test campaign including uniaxial and equibiaxial experiments. Our data can be used to derive model equations for IPN membranes. Different from all previous attempts we determined parameter simultaneously for uni- and biaxial stress states, for different loading profiles and deformation histories. This is of fundamental importance to predict the materials response in a wide range of strain states and strain rate.

In general the determination of stress values from biaxial tensile tests with cruciform specimens requires a FE simulation due to the inhomogeneous stress field. The application of a special cruciform specimen design allows a simplified approach of stress determination, avoiding a computationally costly solution of the inverse problem. The application of simplified models also leads to separate solutions for the uniaxial and biaxial domain in each sample, thus providing information on the strain energy of different kinematic states for the same membrane. We consider this as a major advantage especially for the characterization of materials with strongly varying properties like composites or biological tissue.

We further characterized the influence of the process induced variations of mechanical response which was found to be very pronounced. As can be seen in Fig. 9 samples tested under nominally identical conditions reveal up to 15% difference in their response. One and the same material model can therefore not predict the behavior of all samples despite very similar conditions of imposed strain or strain rates. The material model was therefore extended with a membrane specific correction factor and the undeformed membrane thickness, which is easy to measure, was selected as the variable used to describe the value of the membrane specific parameter. The proposed thickness dependent correction of the strain energy density function represents a phenomenological approach that was found useful for fitting the presented experimental data from membranes of different thickness. After introducing the membrane specific correction function the model well predicts the material behavior in all experiments for different values of strain, strain rate and stress state (different locations in the specimen).

The predictive capabilities of a phenomenological model with respect to different conditions of (multiaxial) stress can only be evaluated using corresponding experimental configurations. The Ogden form used in this work was shown to predict well the response under uniaxial and equibiaxial stress states. Furthermore, in [37] we applied the same model for the analysis of so called “inflation experiments” with IPN membranes of different material composition. The model successfully predicts the behavior of an inflated membrane for samples with a similar thickness than the ones tested in this work, under conditions ranging from pure shear to equibiaxial stress.

While the method was shown to provide satisfactory results for all membranes investigated in this study, the validity of this approach should be verified in future work

with a statistical evaluation of the mechanical variability of IPN membranes with identical thickness. Physically based formulations accounting for the interaction of two polymer networks, such as in the model proposed by Zhu and Suo [21], might be developed using the data reported in this paper. One should consider, however, that material composition is not the only factor influencing the mechanical behavior of IPN. Other variables like the curing temperature profile, variations in reactivity of TMPTMA due to aging, or the properties of the VHB membrane might significantly affect the properties of the IPN membrane.

This work characterizes the response of IPN membranes at room temperature. It should however be considered that, in many possible applications of DEA temperature related effects might become important. Not only the mechanical properties will change with temperature, but also the electromechanical behavior (resistivity, permittivity) and the mechanism leading to actuator deterioration and failure. Future experimental work is required to address these issues.

Acknowledgement Financial support from the Swiss National Science Foundation (Project Nr. 200021-107661) is gratefully acknowledged.

References

1. Kofod G, Sommer-Larsen P, Kornbluh R, Pelrine R (2003) Actuation response of polyacrylate dielectric elastomers. J Intell Mater Syst Struct 14:787–795
2. Kofod G (2008) The static actuation of dielectric elastomer actuators: how does pre-stretch improve actuation? J Phys D Appl Phys 41:215405
3. Corbett D, Warner M (2009) Anisotropic electrostatic actuation. J Phys D Appl Phys 42:115505
4. Ha SM, Yuan W, Pei Q, Pelrine R, Stanford S (2006) Interpenetrating polymer networks for high-performance electroelastomer artificial muscles. Adv Mater 18:887–891
5. Kovacs G, Düring L, Michel S, Terrasi G (2009) Stacked dielectric elastomer actuator for tensile force transmission. Sens Actuators A 155:299–307
6. Kofod G (2001) Dielectric elastomer actuators. PhD-thesis, Riso-R-1286 (EN)
7. Carpi F, De Rossi D (2004) Dielectric Elastomer cylindrical actuators: electromechanical modeling and experimental evaluation. Mat Sci Eng C 24:555–562
8. Goulbourne N, Mockensturm NE, Frecker M (2005) A nonlinear model for dielectric elastomer membranes. J Appl Mech 72:899–906
9. Lochmatter P, Michel S, Kovacs G (2006) Electromechanical model for static and dynamic activation of elementary dielectric elastomer actuators. Proc. SPIE, 6168
10. Sommer-Larsen P, Kofod G et al (2002) Performance of dielectric elastomer actuators and materials. Proc SPIE 4695:158–166
11. Wissler M, Mazza E (2005) Modeling and simulation of dielectric elastomer actuators. Smart Mater Struct 14:1396–1402
12. Ha MS, Wissler M, Pelrine R, Stanford S, Kovacs G, Pei Q (2007) Characterization of electroelastomers based on interpenetrating polymer networks. Proc. SPIE, 6524
13. Yang E, Frecker M, Mockensturm E (2005) Viscoelastic model of dielectric elastomer membranes. Proc SPIE 5759:82–92
14. Plante JS (2006) Dielectric elastomer actuators for binary robotics and mechatronics. Ph.D. Thesis, Department of Mechanical Engineering, Massachusetts Institute of Technology, Cambridge, MA
15. Plante JS, Dubowsky (2006) Large-scale failure modes of dielectric elastomer actuators. Int J Solids Struct 43:7727–7751
16. Wissler M, Mazza E (2007) Mechanical behavior of an acrylic elastomer used in dielectric elastomer actuators. Sens Actuators A 134:494–504
17. Pelrine RE, Kornbluh RD, Joseph JP (1998) Electrostriction of polymer dielectrics with compliant electrodes as a means of actuation. Sens Actuators A 64:77–85
18. Zhao X, Suo Z (2008) Electrostriction in elastic dielectrics undergoing large deformation. J Appl Phys 104:123530
19. Ha SM, Yuan W, Pei Q, Pelrine R, Stanford S (2007) Interpenetrating networks of elastomers exhibiting 300 % electrically-induced area strain. Smart Mater Struct 16:280–287
20. Düring L (2008) EAP stack actuator. Master thesis. Department of Mechanical and Process Engineering, Swiss Federal Institute of Technology Zurich ETHZ, Switzerland
21. Zhu J, Suo Z (2009) Dielectric elastomers of interpenetrating networks. Appl Phys Lett 95:1
22. Rivlin RS, Saunders DW (1951) Large elastic deformations of isotropic materials VII. Experiments on the deformation of rubber. Philos Trans R Soc A 243(865):251–288
23. Mönch E, Galster D (1963) A method for producing a defined uniform biaxial tensile stress field. Br J Appl Phys 14:810–812
24. Lanir Y, Fung YC (1974) Two-dimensional mechanical properties of rabbit skin I. Experimental System. J Biomech 7:29–34
25. Makinde A, Thibodeau L, Neale KW (1992) Development of an apparatus for biaxial testing using cruciform specimens. Exp Mech 32(2):138–144
26. Sacks MS (2000) Biaxial mechanical evaluation of planar biological materials. J Elast 61:199–246
27. Waldmann SD, Lee JM (2002) Boundary conditions during biaxial testing of planar connective tissues. Part 1: Dynamic behavior. J Mat Sci: Mater Med 13:933–938
28. Grashow JS, Sacks MS (2006) Biaxial stress-stretch behavior of the mitral valve anterior leaflet at physiologic strain rates. Ann Biomed Eng 34:315–325
29. Gundia N, Pruitt LA (2007) Determination of strain energy function for arterial elastin: experiments using histology and mechanical tests. J Biomech 40:586–594
30. Helfenstein J, Hollenstein M, Mazza E (2009) Investigation on the optimal specimen design for planar-biaxial materials testing of soft materials. Proc. 6th Eur. Conf. Const. Models for Rubber, 371-376
31. Anderson IA, Hale T, Gisby T, Inamura T, McKay T, O'Brien B, Walbran S, Calius EP (2010) A thin membrane artificial muscle rotary motor. Appl Phys A 98:75–83
32. Jordi C, Michel S, Fink E (2010) Fish-like propulsion of an airship with planar membrane dielectric elastomer actuators. J Bioinsp Biomim 5:026007
33. Yeoh OH (1993) Some forms of the strain energy function for rubber. Rubber Chem Technol 66:754–771
34. Ogden RW (1972) Large deformation isotropic elasticity – on the correlation of theory and experiment for incompressible rubberlike solids. Proc R Soc Lond A 326:565–584
35. Arruda EM, Boyce MC (1993) A three-dimensional constitutive model for the large stretch behaviour of rubber elastic materials. J Mech Phys Solids 41:389–412
36. Lagarias JC, Reeds JA, Wright MH, Wright PE (1998) Convergence properties of the Nelder-Mead simplex method in low dimensions. SIAM J Optim 9(1):112–147
37. Schmidt A, Bergamini A, Kovacs G, Mazza E (2010) Mechanical modeling of Interpenetrating Polymer Network reinforced acrylic elastomer, Proc. SPIE, 76421O-1